© January 2025 | IJIRT | Volume 11 Issue 8 | ISSN: 2349-6002

Harmonic Analysis of Deep Groove Ball Bearing with Multiple Surface-Defects Using Finite Element Method.

Shivam S. Dingane[1], Amar Namdeo Adsul[2]

[1]*Head of Mechanical Engineering Department, Smt Premalatai Chavan Polytechnic, Karad, Satara.*

[2]*Lecturer, Department of Mechanical Engineering, Abhaysinharaje Bhonsle institute Of Technology Shendre Satara. Maharashtra, India*

***Abstract*—Monitoring vibration is essential for evaluating the health of rotating systems. Undetected faults in these systems can cause breakdowns, extensive damage, injuries, or even fatalities. Therefore, early fault detection is vital to ensure the longevity and smooth operation of rotating machinery. Bearings, which are crucial components in these systems, support rotating shafts and are susceptible to various types of vibrations during use. These vibrations can reduce performance and compromise safety, leading to downtime and expensive repairs if not addressed. Defects or malfunctions in bearings can cause misalignment, equipment damage, and hazardous conditions. As a result, fault diagnosis has become a key focus for researchers. By measuring and analyzing bearing vibrations, critical issues like mass unbalance, misalignment, surface defects, and cracks can be detected and addressed. This article aims to guide researchers in using vibration analysis to identify, diagnose, and resolve common faults. It also discusses important techniques for condition monitoring of deep groove ball bearings, including fast Fourier transform and finite element methods (FEM). The study specifically investigates the modal and harmonic response of deep groove ball bearings with multiple surface defects.**

***Index Terms*—Deep Grove Ball Bearings; Finite Element Technique; Modal Analysis, Harmonic Analysis.**

I. INTRODUCTION

Between 5000 BC and 3000 BC, wheeled vehicles equipped with simple bearings became prevalent. The earliest recorded instance of a rolling element bearing is found in the wooden ball bearing supporting the rotating table recovered from the Roman Nemi shipwreck in Lake Nemi, Italy, dating back to 40 BC. Philip Vaughan, a British inventor and iron master, obtained the first recognized modern patent for ball bearings in 1794, developing the initial design to support a carriage axle. Bearings represent a crucial component within any rotating mechanism, providing essential support for spinning shafts in machinery. Consequently, any malfunction or fault in the bearings can lead to production losses, equipment damage, and hazardous working conditions for personnel. Thus, bearing fault diagnosis has garnered significant attention from researchers in recent years, employing techniques such as time domain analysis, frequency domain analysis, and spike energy analysis to identify various bearing faults. Vibration analysis stands as a key parameter in the condition monitoring of rotating systems. Undetected faults within these systems can result in downtime, costly damages, injuries, or even fatalities, underscoring the critical importance of early fault detection in preserving and prolonging the operational lifespan of rotating systems. Bearing failures can have wide-ranging consequences for facilities, including increased downtime, elevated maintenance expenses, delivery delays, revenue losses, and potential harm to workers. Finite Element Analysis (FEA) involves using calculations, models, and simulations to predict how an object will behave under different physical conditions. Modal analysis assesses the vibration response of a structure, determining its natural or resonant frequencies empirically or theoretically. These frequencies provide insight into the operational frequency range of a component. Harmonic Response Analysis, also known as Frequency Response Analysis, is a linear dynamic analysis method used to evaluate a system's response to excitation at specific frequencies. In this analysis, the load applied to the linear model is a steady-state sinusoidal load at a predetermined frequency. While loads may be out of phase with each other, the excitation frequency is known. Modal and Harmonic Response analyses are conducted on bearings with multiple surface defects at various operating speeds.

Dipen S. Shah et al. [1] have endeavored to illustrate the process of modeling and simulating local and distributed defects on the inner and outer races of deep groove ball bearings. They represent the bearing defects as impulse train forces or impact forces, inducing additional deflection or excitation of the rolling elements. The simulated outcomes have been scrutinized in both the time and frequency domains. The simulated results extensively explore the characteristic defect frequency, its harmonics, and the amplitude of vibration response in the defective bearing.

Suryawanshi G. L. et al. [2] explored how inclined surface faults affect the dynamic response of rolling element bearings. They developed a dynamic model through dimensional analysis and conducted experimental investigations on the vibration responses of double row spherical roller bearings. The goal was to analyze how the size and slope angle of artificially induced inclined surface faults impact the bearings. The findings indicated that as the inclination angle of the surface fault increased, the relative vibration amplitude decreased at various rotor speeds, but increased with fault depth. Abhay Utpat [3] constructed a model representing the bearing system as a spring-mass system, with races considered as masses and balls as springs. This approach was further developed by employing Finite Element Analysis to investigate the peaks corresponding to defect frequencies on both the outer and inner rings of the bearing. To validate the numerical findings, actual vibration amplitudes of bearings with simulated local defects were measured, demonstrating strong alignment with the numerical results. Standard support bearings were consistently utilized throughout the experimentation process. V. N. Patel et al. [4,11] presented a dynamic model aimed at investigating the vibrations of deep groove ball bearings afflicted with single or multiple defects on the surfaces of their inner and outer races. The model incorporates the masses of the shaft, housing, races, and balls. Employing the Runge-Kutta method, the model provides a coupled solution for the governing equations of motion. It furnishes vibrations of the shaft, balls, and housing across both time and frequency domains. The computed results obtained from the model were compared against experimental findings, which involved healthy and defective deep groove ball bearings. The study also encompassed theoretical and experimental analyses of dynamically loaded deep groove ball bearings with local circular defects on either race. The mathematical model includes masses of the shaft, housing, raceways, and balls. Similarly, the Runge-Kutta method was utilized to attain coupled solutions for the governing equations of motion. The model offers vibration responses for the shaft, balls, and housing in both time and frequency domains. Validation of the results obtained from the proposed mathematical model was conducted against experimental outcomes. During experiments, the test bearings were subjected to radial loading using an electro-mechanical shaker, with radial load excitation frequencies ranging from 10 to 1000. Hz. Laxmikant G Keni et al. [5] have presented a reliable procedure for accurately identifying deformities in bearing components. They conducted amplitude measurements of vibrations at 5000 RPM and a load of 200 N, considering different deformity sizes of 3 mm and 4 mm on bearing races. An initial vibration analysis of the rolling component was performed using Ansys R-18.0. Vibration signals corresponding to two different defect sizes were extracted, and a reference file for comparing various defect sizes was proposed. The study also investigated the effects of radial load, rotation speed, and initial defect size on stress levels.

Sameera Mufazzal et al. [6] offer a comprehensive examination of the vibration response in ball bearings through a modified 2-degree of freedom (DOF) lumped parameter model. This model integrates additional deflection and multi-impact theories to closely replicate the behaviour of both healthy and defective bearings across varying load and speed conditions. The study delves into the intricacies of varying compliance vibrations, revealing that the location and number of impulses resulting from varying compliance are significantly influenced by multiple factors, particularly the applied load and shaft rotational speed. These impulses may merge with the impulses caused by actual defects, potentially altering their characteristics. Numerical simulations were conducted at different speeds, loads, defect sizes, and locations to explore the impact of these parameters on the bearing response characteristics. The paper also presents experimental results and thorough analyses to support the proposed model and validate the numerical findings.

J. Sopanen et al. [7,8] introduced a dynamic model for a deep-groove ball bearing featuring six degrees of freedom. Input parameters such as geometry, material properties, and diametral clearance of the bearing are provided for the model. The force and torque exerted on the bearing are calculated based on the relative displacements and velocities between the bearing rings. Both distributed defects, like inner and outer ring waviness, and localized defects, such as inner and outer ring defects, are accounted for in the model. The model proposed in Part 1 is implemented and analyzed using a commercial multi-body system software application (MSC.ADAMS). The impact of the bearing's diametral clearance on the natural frequencies and vibration response of the rotor–bearing system is investigated. It's observed that the diametral clearance significantly influences the vibration level and natural frequencies. Low-order waviness, known as out-of-roundness, causes vibrations at frequencies that result from multiplying the order of waviness by the rotation speed. Conversely, waviness orders close to the number of balls in the bearing ($z \pm 1$ and z) generate vibrations at the frequencies associated with the passage of balls through the inner and outer rings. TANG Zhaoping et al. [9] constructed a three-dimensional model of a deep groove ball bearing using the APDL language integrated into the finite element software ANSYS. By conducting contact analysis, they were able to visualize changes in stress, strain, penetration, sliding distance, and friction stress among the inner ring, outer ring, rolling elements, and cage. Additionally, the simulation outcomes indicated that the computed values aligned with theoretical expectations. These findings collectively affirm the accuracy and validity of the model and its associated boundary conditions, offering a solid foundation for the optimal design of rolling bearings under complex loads. Viramgama Parth D. et al. [12] conducted an analysis of ball bearings using finite element analysis to examine the stress levels and displacement behavior of the bearings. Their primary objective was to identify the parameters that most significantly affect the radial stiffness of the bearing under axial loads. The analysis focused on a specific single-row deep groove ball bearing with an outer diameter of 170 mm, inner diameter of 80 mm, and ball diameter of 28.575 mm. These bearings are utilized to support loads and facilitate relative motion within mechanical systems. Through this analysis, they aimed to assess factors such as the bearing's lifespan, rejection rate, and productivity. Ghasem Ghannad Tehrani et al. [13] conducted stability analysis on a ball bearing system that incorporates varying stiffness coefficients. The presence of variable stiffness can lead to instabilities within the system at specific combinations of rotational speed, number, and dimensions of balls, thereby complicating the design process. The primary objective is to determine the stability boundary curves (SBCs) that delineate the stable and unstable regions. The well-known Mathieu equation serves as the governing equations of the system in both horizontal and vertical directions. While this process is straightforward for uncoupled Mathieu equations, whether damped or undamped, a realistic bearing system typically requires the consideration of two coupled Mathieu equations, introducing two dominant frequencies that are not integer coefficients of each other. This more complex, damped, and coupled set of equations applied to a bearing system is solved using HBM for the first time, avoiding the need for costly iterative methods. The accuracy of all examined cases, including uncoupled-undamped, uncoupled-damped, and coupled-damped, is ensured through Floquet Theory. Wyatt Peterson et al. [14] employed ANSYS FLUENT computational fluid dynamics (CFD) software to create a comprehensive model of single-phase oil flow within a deep groove ball bearing (DGBB). The CFD model was utilized to examine fluid flow characteristics in relation to bearing geometry and operational conditions. The paper provides detailed explanations of the underlying theory, boundary conditions, and model development. Key aspects of the model, including meshing techniques, mesh density, and geometric clearances, were determined through parametric studies. Streamlines, velocity vectors, and pressure contours were examined to investigate different aspects of DGBB, including cage design and properties of the lubricant. The developed CFD model offers a novel approach for studying DGBB fluid flow dynamics and assessing the impact of cage geometry on bearing performance. Iker Heras et al. [15] discussed the advantages of wire race bearings, including weight and inertia reductions, effective shock load and vibration absorption, consistent torque, and minimal maintenance requirements.

II. FINITE ELEMENT METHOD

2.1 Modeling of Deep Groove Ball Bearing

The 3D model with two and three surface defects have been developed to analyze the frequency response and compare the results with healthy bearing.

1.1.1. Bearing Specifications

Table No. 1 Dimensions of 6206 SKF deep groove ball bearing [15]

Dimensions	
Bore diameter (d)	30 mm
Outside diameter (D)	62 mm
Pitch Circle diameter	46 mm
Width (B)	16 mm
Roller diameter	10.4 mm
Ball Number	09
Mass of bearing	0.2kg

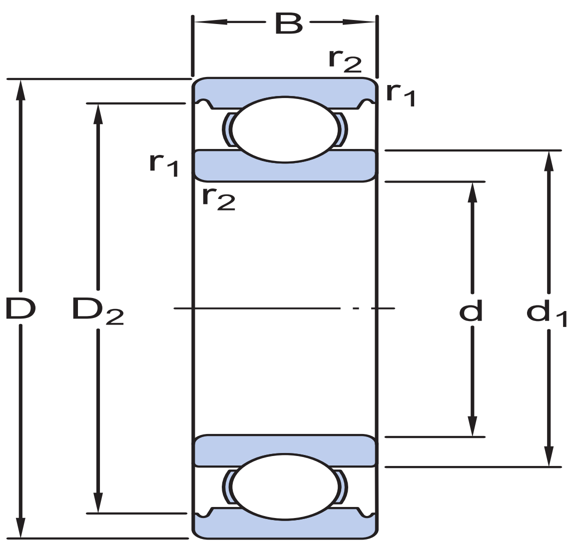

Figure 1. Illustrated Dimensions of 6206 Ball Bearing [15]

The whole bearing is made of Stainless steel, hence the properties of stainless steel are given below

Table No. 2 Mechanical Properties of Stainless steel [16,17,18]

Properties	Value
TensileYieldStrength(MPa)	207
UltimateYield Strength(MPa)	586
Density(kg/m3)	7750
Young'sModulus(MPa)	1.93E+05
Poisson'sRatio	0.31
BulkModulus(MPa)	1.693E+05

Geometric Model

The two 3-Dimensional geometric models are developed using Creo Parametric 5.0.6.0 with two and three surface-defects of 2x2 mm on the outside of inner race respectively

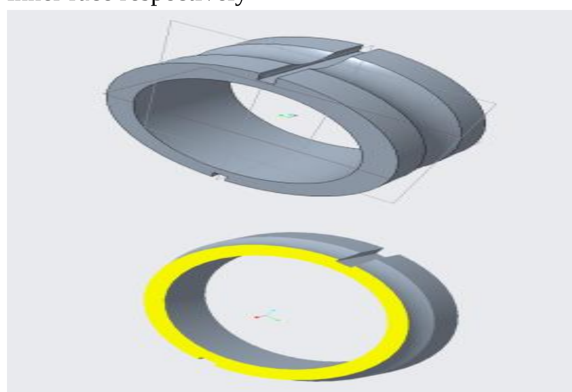

(a) (b)

Figure 2

Figure 2(a). Wireframe 3D model of inner race with two surface defects at an instant of 180°.

Figure 2(b). Section view of inner race.

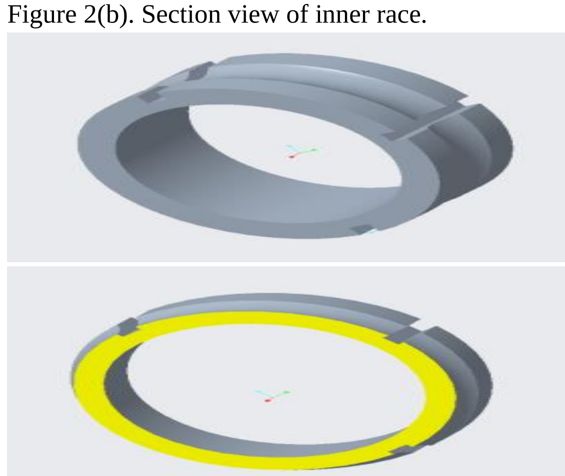

(a) (b)

Figure 3

Figure3(a). 3D model of inner race with three surface defects at an instant of 90º.
Figure 3(b). Section view of inner race.

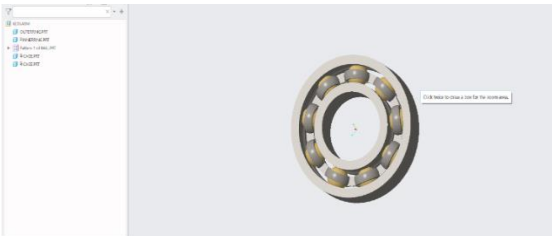

Figure 4. 3D Model of Deep Groove Ball bearing

The above figure shows the complete assembly of deep groove ball bearing which includes Outer race, Inner race with two and three defects, balls and cage. The model will be used to perform frequency response analysis.

1.1. Rotar Dynamics Equation

The General equation is given by

$[M]\{\ddot{\mu}\} + [c]\{\dot{\mu}\} + [K]\{\mu\} = \{f(t)\}\ldots$ (1)

[M], is the mass matrix [C], is the damping matrix and [K] is the stiffness matrix, and {f} is the external vector force, In the rotor dynamics, this equation gets additional contributions from the gyroscopic effect [G], and the rotating damping effect [B] leading:

$[M]\{\ddot{\mu}\} + ([C] + [G]\{\dot{\mu}\}) + ([K] + [B])\{\mu\} = \{F(t)\}$...(2)

In modal analysis the mode shapes and natural frequencies with them are one of the characteristics of the mechanical structure, regardless of any loads, what we do is an undamped vibration system, so the external excitation and damping are not taken into account in the model analysis, and from it, the equation (2) can be simplified as follows:

$[M]\{\ddot{\mu}\} + ([K] + [B])\{\mu\} = \{0\}\ldots(3)$

The free vibration of an elastic body can always be decomposed into a series of simple harmonic vibrations, that is, it can be assumed that each point in the structure experiences a harmonic motion that can decrease due to frequency, amplitude, and phase angle. The equation is simplified to:

$$(([K] - [B]) - \omega_i^2[M])\{\emptyset\}_i = 0 \qquad (4)$$

is the eigenvalue, is the eigenvector, So, the equation for free vibration becomes:

$|([K] - [B]) - \omega_i^2[M])| = 0\ldots(5)$

is the natural frequency of the mode shape.

For harmonic response the equation of forced vibration is given by:

$[M]\{\ddot{\mu}\} + [c]\{\dot{\mu}\} + [K]\{\mu\} = \{f(t)\}$**...(**6)

$f(t) = f_0 \sin \omega t\ldots(7)$

1.2. Finite Element Model

The Ansys R1 workbench software is used to perform finite element modelling and obtaining the results in the form of Natural Frequencies, mode shapes and Campbell diagram [19,20]

2.3.1 Boundary Conditions

The same boundary conditions are applied to all the models with 2 and 3 surface-defects and healthy bearing.

2.3.2 Connections and Joints

The connections of the components of the ball bearing which includes the contact between balls and outer race and balls and inner race. By considering Ideal condition these contacts are defined are frictionless.

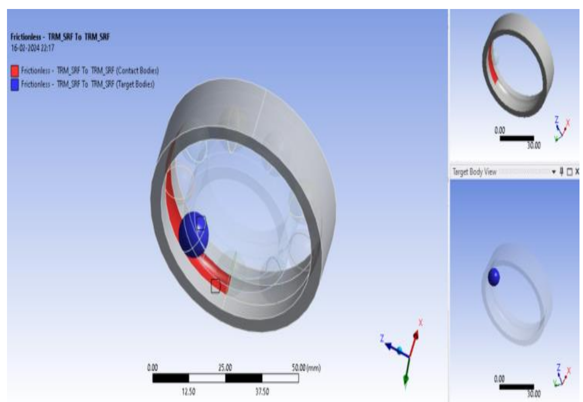

Figure 5 **–** Contact between anyone ball and outer race

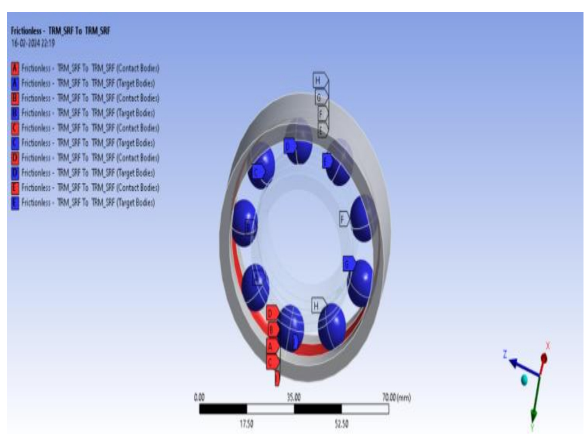

Figure 6 – Contact between the balls and outer race

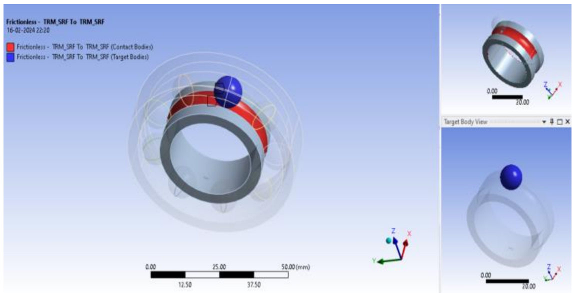

Figure 7 –Contact between anyone ball and inner-race

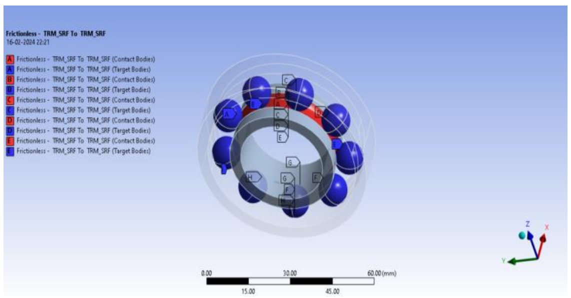

Figure 8 –Contact between the balls and inner race

The total number of 18 frictionless connections are defined where nine connections are between balls and outer and other nine connections are between balls and inner race.

The joints between the components of deep groove ball bearing are also defined in the connection tab, the revolute joint is defined for the inner race and balls where it permits rotation only in one direction i.e., Z.

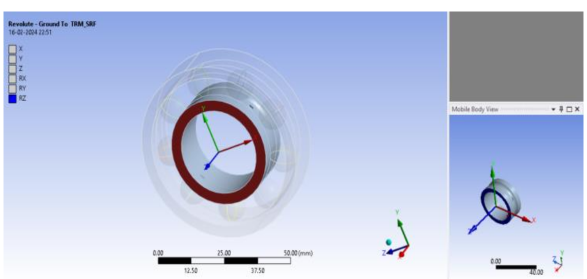

Figure 9 – Inner race defined as revolute joint

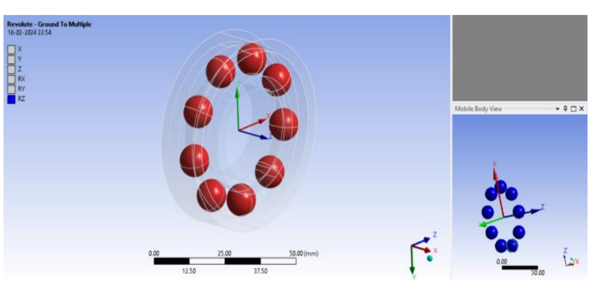

Figure 10 – Bearing balls defined as revolute joint

2.3.3 Boundary Conditions for Modal Analysis

We provide the condition of remote displacement to the ball bearing location to constraint the motion of bearing in the Z axis direction, the translation degrees of freedom are also restricted in the direction of Z axis.

The given maximum speed of bearing is 15000 rpm and the reference speed of bearing is 24000 rpm (revolutions per minute) [15] as per SKF bearing specifications. The modal analysis is carried out in three steps with three different speeds of 500, 600&700 rpm for obtaining mode shapes and 2000, 15000 & 24000 for Campbell Diagram.

The outer race is considered as fixed support where actually the bearing is mounted or fixed, and the rotational velocity is provided to the inner race where it is mounted on shaft.

Analysis Setting are as follows - 4 number of modes to find and the solution system used is damped solver with full damped type and Coriolis effect turned on also Campbell diagram with 3 number of points.

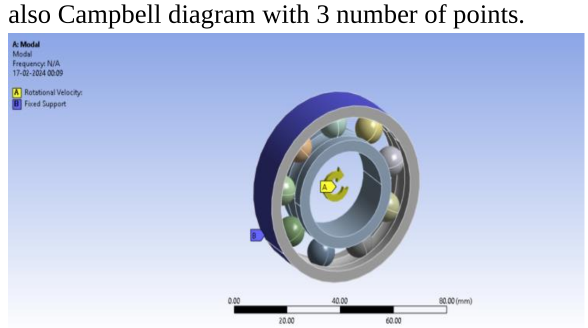

Figure 11 – Rotating velocity and fixed support applied

2.3.4 Boundary Conditions for Harmonic Response

We use the condition of remote displacement to the deep groove ball bearing where the constraint is put on the rotational and transition degrees of freedom in the direction of the Z-axis at bearing sites

The fixed support is applied to the outer race whereas the rotational velocity is provided to the inner race. The rotational velocity (in rpm) is converted to Relative Centrifugal force (RCF in Newtons). The conversion is given by

$$\mathrm{RCF} = 1.12 \times r\,(\mathrm{RPM}/1000)^2 \qquad (8)$$

Where RCF is the Relative Centrifugal force and r is the radius of rotating component.

Therefore, to obtain the speed of 700 rpm, the equation no. 8 is modified according to the values of the bearing

$$\therefore \mathrm{RCF} = 1.12 \times 31\,(700/1000)^2 \qquad (9)$$

$$\therefore \text{RCF} = 17.01 \text{ N} \quad (10)$$

The RCF of 17.01N is applied to the inner race at the remote point created for the location of hit point.In the analysis settings the frequency range were defined from 0 to 1000 Hz.

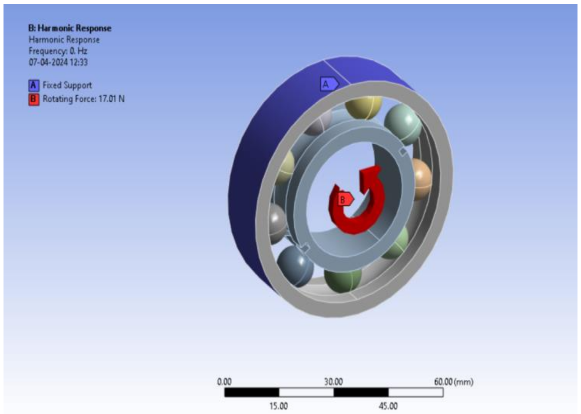

Figure 12 – Appliedrotating force and fixed support applied

2.3.5Meshing

ANSYS's meshing method plays an essential role for accurate simulation utilizing Finite Element Analysis (FEA). The mesh is made up of elements with nodes that represent the shape of the geometry and can vary depending on the element type. FEA reduces degrees of freedom from unlimited to limited by performing calculations at a finite number of elements and interpolating the results to the full size of a continuous object. The ANSYS workbench offers a variety of meshing methods, including mechanical.

The average surface area covered 297.29 mm². A total number of 65554 elements are created and 166313 nodes are shown in the below figure

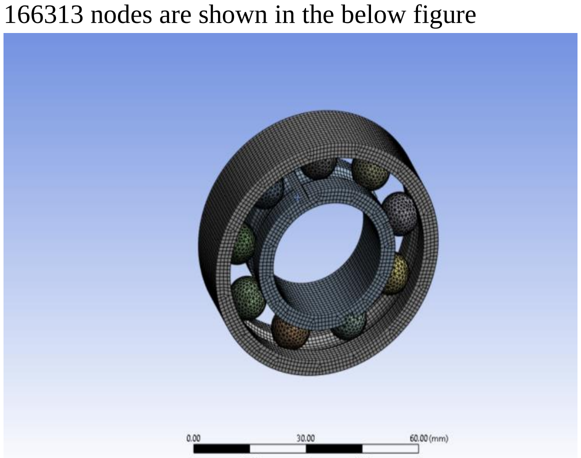

Figure 13 – Bearing Mesh

III. EXPERIMENTAL METHOD

3.1 Experimental Setup

The experimental setup comprises a DC motor capable of adjusting its speed, along with a shaft, loading mechanism, speed controller, FFT analyzer, coupling, bearing housing, accelerometer, and proximity sensor. The ADC motor within the experiment can rotate within a range of 0 to 3000 rpm. The shaft is equipped with keyways, steps, and mounting locations for bearings, while a bearing housing is employed to secure the bearings. Additionally, a flexible coupling is utilized to transfer torque from the drive system to the shaft, enabling it to operate with slight variations.

Figure 14 – Experimental Setup

An accelerometer is an instrument used to measure the vibration or acceleration of movement in a structure. It operates on the principle of piezoelectricity, where the material within is compressed by the mass due to vibrational force or changes in velocity (acceleration). This compression generates an electrical charge that correspond ds to the applied force. Given that the mass remains constant and the charge is directly proportional to the force, it follows that the charge is also directly proportional to the acceleration. Therefore, an accelerometer is a tool designed to gauge the vibration or acceleration of a structure.

Figure 15 – Bruel and Kjaer FFT

In the realm of vibration analysis, the "Fast Fourier Transform" (FFT) serves as a fundamental technique for measurement. It dissects a signal into its constituent spectral components. FFTs find applications in machine or system condition monitoring, quality control, and fault analysis. This article elucidates the functionality of FFT, the relevant parameters involved, and their impact on measurement outcomes. Essentially, the "Discrete Fourier Transformation" is practically executed through an optimized algorithm known as the FFT (DFT). This process involves segmenting a signal into its frequency constituents post-sampling over time. Each of these constituents represents a single sinusoidal oscillation characterized by a distinct frequency, amplitude, and phase. Type 3050-B-0404inch, Input Module with a sampling frequency of 50kHz. Fig. 15 shows Bruel and Kjaer FFT.

Figure 16 – Bearings with Defect

6206 Deep groove ball bearings were used to perform the experiment, the artificial defects were made on the same ball bearing using Wire cut Electro discharge Machining (W-EDM) method. Tests were carried out for 500, 600 and 700 RPM respectively without applying load.

IV. RESULTS AND DISCUSSION

4.1 Modal Analysis of Ball Bearing

Modal analysis was carried out for deep groove ball bearing with no surface defects, two surface-defects and three surface-defects. Where we note that first frequency for healthy bearing is 221.74 Hz and the frequency at second mode is way far from the first i.e., 52552 Hz. The first frequency for two surface-defects is 284.7 Hz and frequency at second mode is 32909 Hz. And the frequency at first and second mode of ball bearing with three surface-defects is 287.14 and 32991 respectively

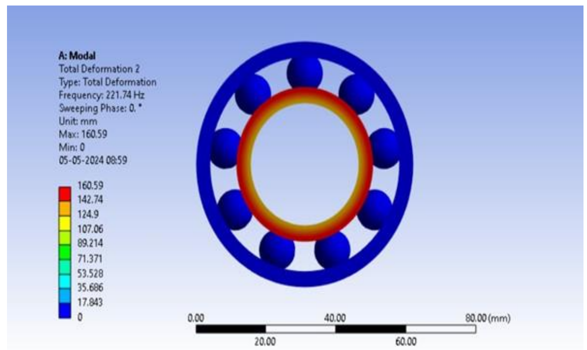

Figure 17 (a)– Mode Shape 1(non-defective)

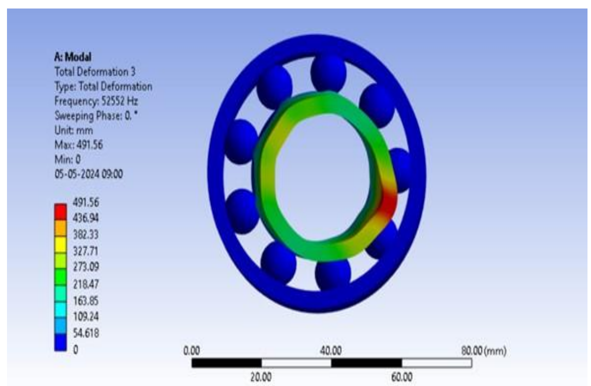

Figure 17 (b)– Mode Shape 2 (non-defective)

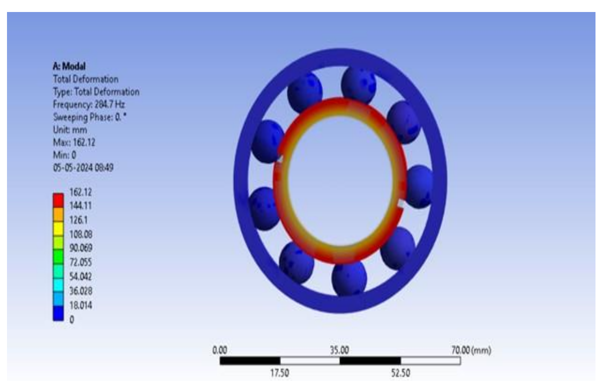

Figure 17 (c)– Mode Shape 1 (two-defects)

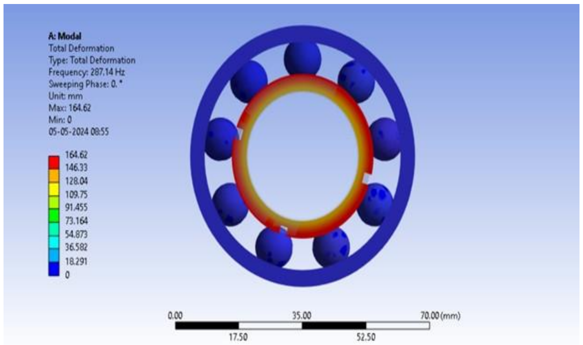

Figure 17 (d)– Mode Shape 2 (two-defects)

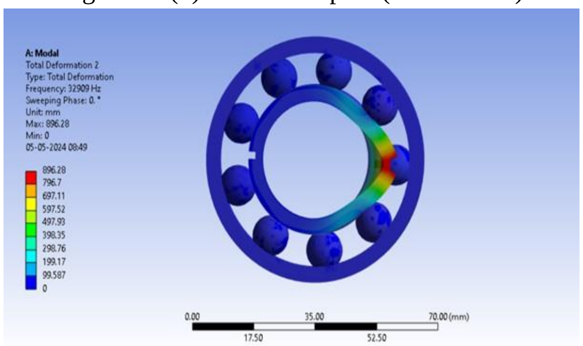

Figure 17 (e)– Mode Shape 1 (three-defects)

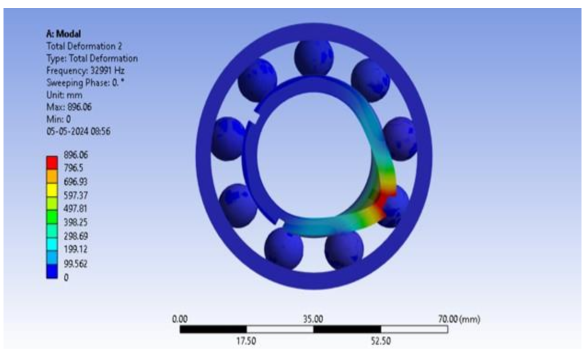

Figure 17 (f)– Mode Shape 2 (three-defects)

4.1.1 Campbell Diagram

We can obtain Campbell diagram as shown in Fig 18 to analyse the evolution of frequencies at the speed of rotation and to determine the critical velocities and stability threshold. In non-defective bearing we note that there is one critical speed of 13304 rpm at 221.74 Hz, and the mode stability is stable. In two-defect bearing we obtain critical speed of 17082 rpm at 284.7 Hz and mode stability is stable in three defective bearing we get the critical speed of 17228 at 287.14 Hz and we have stable mode stability. Figures 18, 19, 20 shows the Campbell diagram for all three bearings.

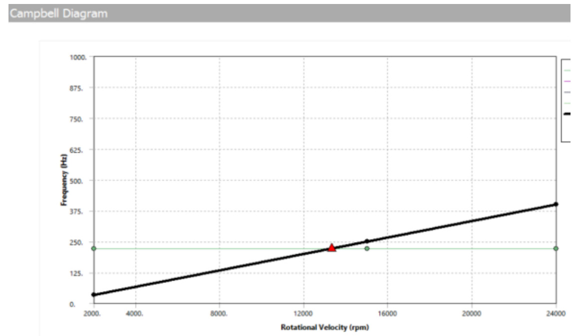

Figure 18 – Campbell Diagram (non-defect)

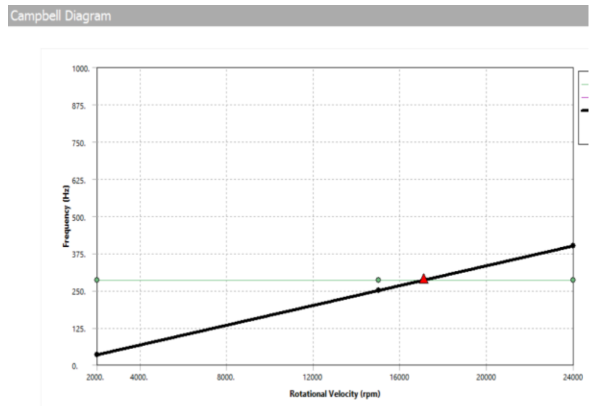

Figure 19 – Campbell Diagram (two-defects)

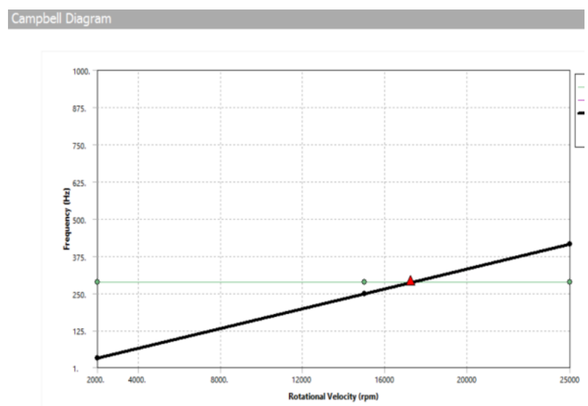

Figure 20 – Campbell Diagram (three-defects)

4.2 Harmonic Response Analysis of Ball Bearing using Finite Element Technique

The harmonic response analysis of the system scope us to determine the deformation, stresses, and effect of phase angle due to balanced and unbalanced forces acting on the bearing system, the harmonic analysis was carried out to show the frequency response by applying a Relative centrifugal force of 17.01 N converted in equation number (10) due to angular velocity of 700 rpm. Similarly, force of 8.68 N and

12.49 N is converted from the speed of 500 and 600 rpm respectively

The frequency response was mentioned on the graph with frequency ranged up to 1000 Hz on X-axis with acceleration as an amplitude in (m/s^2) on Y-axis as shown in figures below in detail. We recorded the maximum amplitude on the frequency of 285.71 Hz, 296.3 Hz, 275.86 Hz at 500, 600, 700 rpm respectively. The figure 21,22,23 shows the plot of natural frequencies of healthy bearing

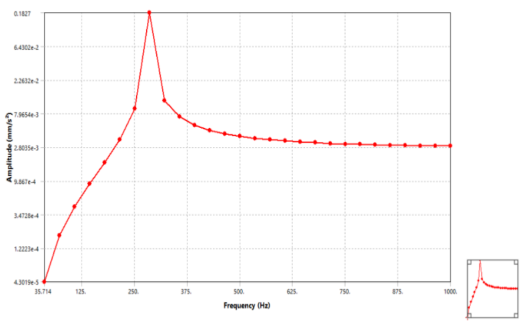

Figure 21 – Frequency Plot ANSYS (500 rpm)

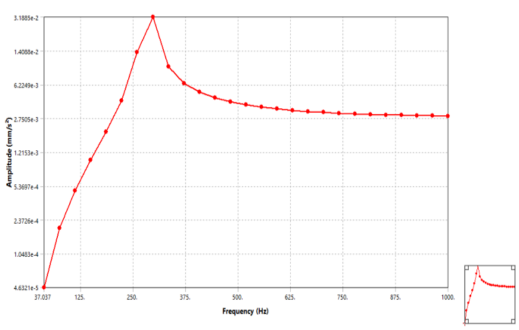

Figure 22 – Frequency Plot ANSYS (600 rpm)

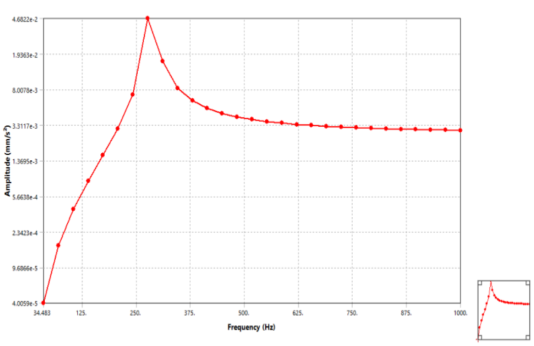

Figure 23 – Frequency Plot ANSYS (700 rpm)

Similarly, we spotted the maximum acceleration on the frequencies of 304.35 Hz, 285.71 Hz and 272.73 Hz, at RPM of 500, 600 and 700 respectively for the bearing with two surface-defects and frequencies of 250 Hz, 260 Hz and 266.67 Hz at 500 rpm, 600 rpm and 700 rpm respectively. As shown in figures no. 24, 25,26, 27, 28, 29 below.

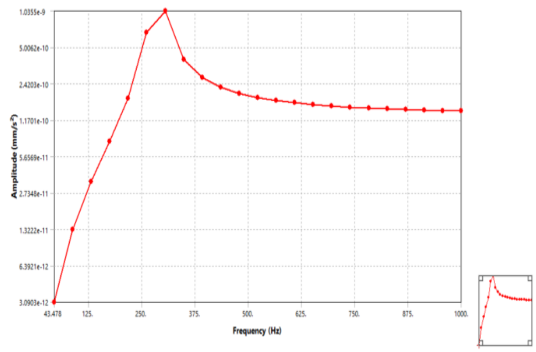

Figure 24 – Frequency Plot ANSYS (500 rpm) (two-defects)

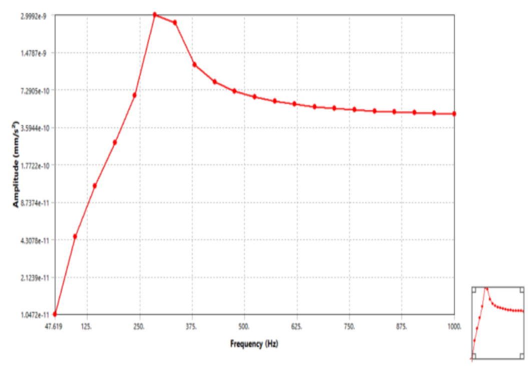

Figure 25 – Frequency Plot ANSYS (600 rpm) (two-defects)

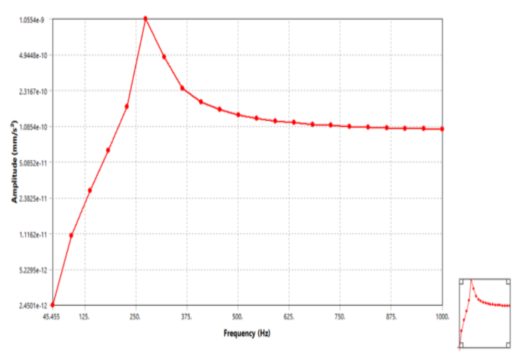

Figure 26 – Frequency Plot ANSYS (700 rpm) (two-defects)

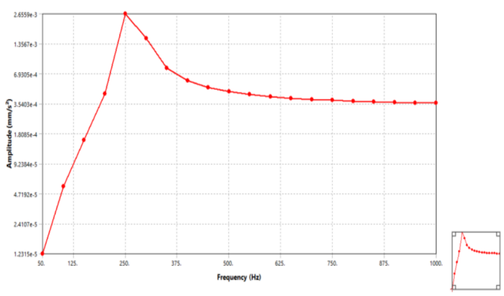

Figure 27 – Frequency Plot ANSYS
(500 rpm) (three-defects)

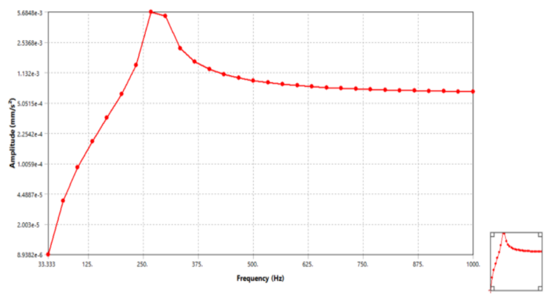

Figure 28 – Frequency Plot ANSYS
(600 rpm) (three-defects)

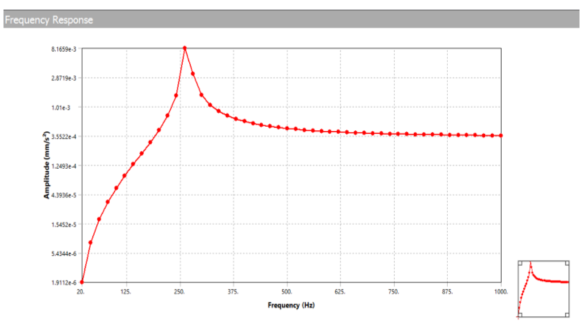

Figure 29 – Frequency Plot ANSYS
(700 rpm) (three-defects)

4.3 Frequency Response Analysis of Ball Bearing by Experimentation

The auto-spectrum was obtained by using FFT analyzer. The graph depicts the frequency response, covering frequencies up to 1000 Hz on the horizontal axis (X-axis) and acceleration, measured in meters per second squared (m/s^2), on the vertical axis (Y-axis). Detailed figures below illustrate this. Notably, maximum amplitudes were observed at frequencies of 242.5 Hz, 247.5 Hz, and 240 Hz corresponding to 500, 600, and 700 rpm, respectively. Figures 30, 31, and 32 present plots showcasing the natural frequencies of a sound bearing.

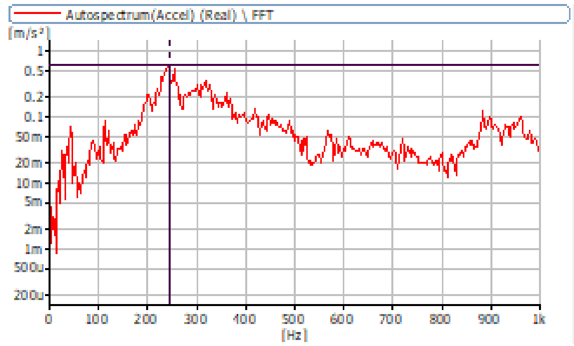

Figure 30 – Frequency spectrum
(500 rpm) (non-defective)

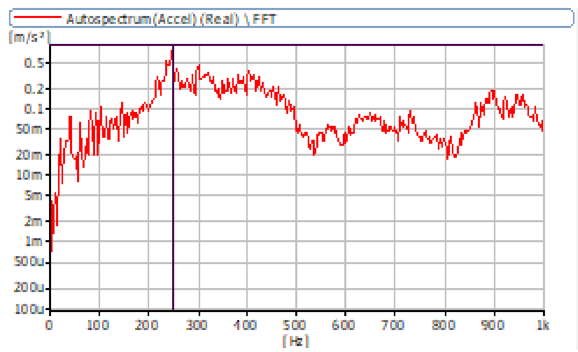

Figure 31 – Frequency spectrum
(600 rpm) (non-defective)

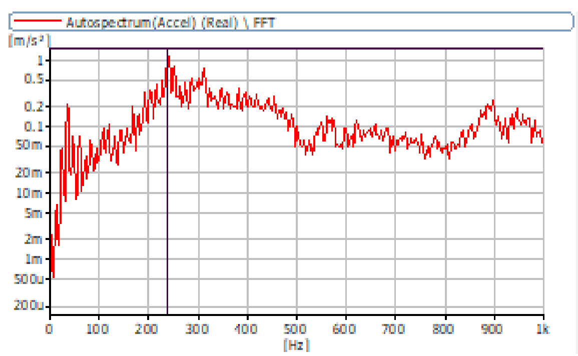

Figure 32 – Frequency spectrum
(700 rpm) (non-defective)

Likewise, we observed peak accelerations occurring at frequencies of 282.5 Hz, 265 Hz, and 262.5 Hz, corresponding to 500, 600, and 700 RPM, respectively, for the bearing exhibiting two surface defects. Additionally, frequencies of 225 Hz, 227.5 Hz, and 292.5 Hz were recorded at 500 RPM, 600 RPM, and 700 RPM, respectively. These findings are illustrated in figures numbered 33 through 38 below.

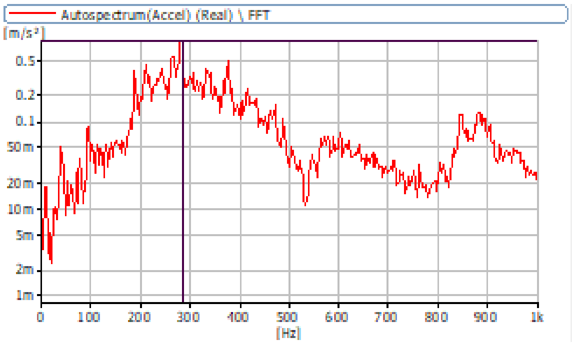

Figure 33 – Frequency spectrum
(500 rpm) (two-defects)

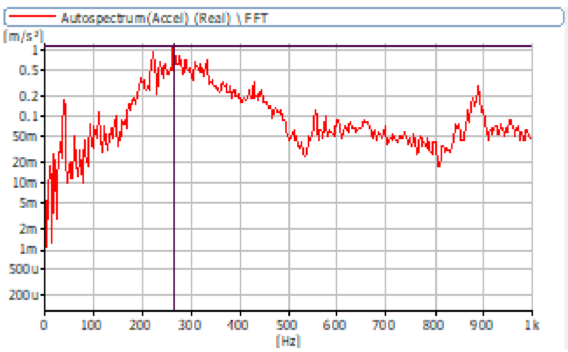

Figure 34 – Frequency spectrum
(600 rpm) (two-defects)

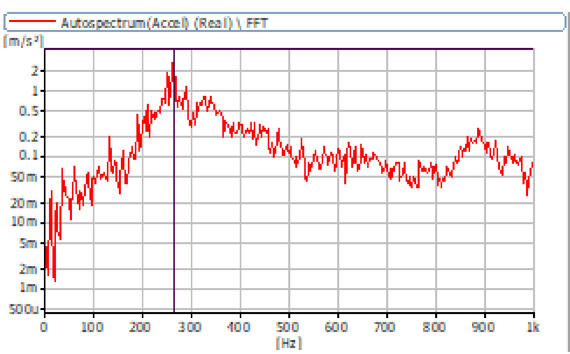

Figure 35 – Frequency spectrum
(700 rpm) (two-defects)

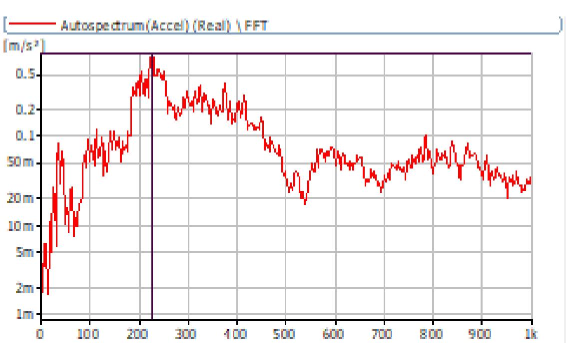

Figure 36 – Frequency spectrum
(500 rpm) (three-defects)

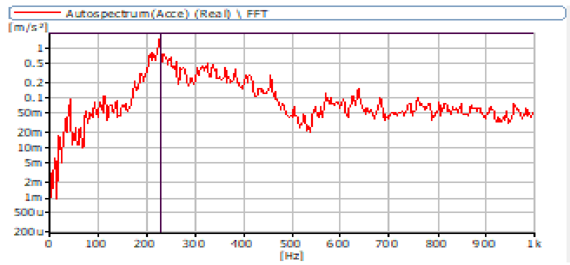

Figure 37 – Frequency spectrum
(600 rpm) (three-defects)

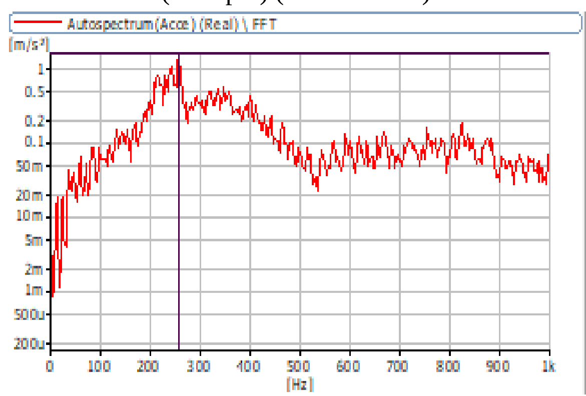

Figure 38 – Frequency spectrum
(700 rpm) (three-defects)

4.3 Discussion

Table no. 3, 4, 5 shows the comparative study of the behavior of bearings with different number of defects.

Table No. 3Comparison between the results of Finite element Technique (FET) and Experimental of Healthy Bearing.

RPM	Frequencies at Maximum Amplitude in (Hz)	
	FET	Experimental
500	285.71	242.5
600	296.3	247.5
700	275.86	240

Table No. 4Comparison between the results of Finite element Technique (FET) and Experimental of Bearing with two surface-defects.

RPM	Frequencies at Maximum Amplitude in (Hz)	
	FET	Experimental
500	304.35	282.5
600	285.71	265
700	272.73	262.5

Table No. 5Comparison between the results of Finite element Technique (FET) and Experimental of Bearing with three surface-defects.

RPM	Frequencies at Maximum Amplitude in (Hz)	
	FET	Experimental
500	250	225
600	260	227.5
700	266.67	257.5

We obtained the mode shapes, Campbell diagram under modal analysis and Frequency response analysis under Harmonic analysis forhealthy and also two and three surface-defects on deep groove ball bearings, The artificial defects were made on bearings to perform actual experimentation to validate the theoretical results. Where we can observer that the frequencies obtained by ANSYS and by empirically at 500 rpm, 600rpm and 700 rpm of healthy bearings shows the same deviation but we also noticesome difference between the results of both methods, can be specified as errors due to human interferences and the environmental conditions. Similarly, the frequencies of bearing with two surface-defects at 700, 600 and 500 rpm are 304.35, 285.71 and 272.73 by FET and 282.5, 265, 262.5 by experimentation where we can see minimum frequency is obtained 700 rpm and maximum at 500 rpm.

V. CONCLUSION

In this research we have carried out the dynamic analysis of deep groove ball bearing with no surface defects, two and three surface defects cause due to improper lubrication, contamination and dirt. We Developed 3D model of deep groove ball bearing using Creo Parametric 5.0.6.0 and performed Modal and Harmonic response analysis using Ansys workbench.

In conclusion, this article offers researchers valuable guidance in utilizing vibration analysis to detect, diagnose, and rectify various common faults. Additionally, it emphasizes the importance of employing essential techniques like fast Fourier transform and FEM for the condition monitoring of deep groove ball bearings. The study's focal point lies in analyzing the modal and harmonic response of deep groove ball bearings afflicted with multiple surface defects.

REFERENCE

[1] Dipen S. Shah, V. N. Patel (2016) “Study on Excitation Forces Generated by Defective Races of Rolling Bearing” Procedia Technology 23 209 – 216.

[2] Ganesh L. Suryawanshi, Sachin K. Patil, Ramchandra G. Desavale,(2021) “Dynamic model to predict vibration characteristics of rolling element bearings with inclined surface fault” Department of Mechanical Engineering, Rajarambapu Institute of Technology, Rajaramnagar, Shivaji University, Kolhapur 415414, Maharashtra, India.

[3] Abhay Utpat (2013) “Vibration Signature analysis of defective deep groove ball bearings by Numerical and Experimental approach” International Journal of Scientific & Engineering Research, Volume 4, Issue 6, June-2013 592 ISSN 2229-5518.

[4] V. N. PatelN. TandonR. K. Pandey, (2019) “A Dynamic Model for Vibration Studies of Deep Groove Ball Bearings Considering Single and Multiple Defects in Races” Industrial Tribology, Machine Dynamic, and Maintenance Engineering Centre (ITMMEC), IIT Delhi, New Delhi 110 016, India.

[5] Laxmikant G Keni, Padmaraj N H, Najiullah Khan, Jagadeesha P E, Pradeep R, Chethan K N (2022) “ANALYSIS OF VIBRATION SIGNATURE IN DEEP GROOVE BALL BEARING USING FINITE ELEMENT METHOD” Paper number: 203, 992, 861-869.

[6] Sameera Mufazzal, SM Muzakkir, Sidra Khanam (2021) “Journal of Sound and Vibration 513

116407 Available online 19 August 2021 0022-460X/© 2021 Elsevier Ltd. All rights reserved.Theoretical and experimental analyses of vibration impulses and their influence on accurate diagnosis of ball bearing with localized outer race defect" Journal of Sound and Vibration 513 (2021) 116407.

[7] J Sopanen and A Mikkola (2003) "Dynamic model of a deep-groove ball bearing including localized and distributed defects." Part 1" DOI: 10.1243/14644190360713551

[8] J Sopanen and A Mikkola (2003) "Dynamic model of a deep-groove ball bearing including localized and distributed defects. Part 2" DOI: 10.1243/14644190360713560

[9] TANG Zhaopinga, SUN Jianping (2011) "The Contact Analysis for Deep Groove Ball Bearing Based on ANSYS" 1877-7058 © 2011 Published by Elsevier Ltd. doi: 10.1016/j.proeng.2011.11.2524

[10] Putti Srinivasa Rao, NariseSaralika, "Thermal and Vibration Analysis of 6200 Deep Groove Ball Bearing" SSRG International Journal of Mechanical Engineering (SSRG-IJME), ISSN: 2348 – 8360.

[11] V. N. Patel, N. Tandon, R. K. Pandey, (2013) "Vibration Studies of Dynamically Loaded Deep Groove Ball Bearings in Presence of Local Defects on Races" Procedia Engineering 64 (2013) 1582 – 1591

[12] Viramgama Parth D. "Analysis of Single Row Deep Groove Ball Bearing", International Journal of Engineering Research & Technology (IJERT)

[13] G.G. Tehrani, C. Gastaldi and T.M. Berruti,(2019) Stability analysis of a parametrically excited ball bearing system, International Journal of Non-Linear Mechanics, doi: https://doi.org/10.1016/j.ijnonlinmec.2019.103350.

[14] Peterson W, Russell T, Sadeghi F, Berhan MT, Stacke L-E, Ståhl J, (2020) A CFD Investigation of Lubricant Flow in Deep Groove Ball Bearings, Tribology International,doi: https://doi.org/10.1016/j.triboint.2020.106735.

[15] SKF Deep Groove Ball bearing 6206, doi: https://www.skf.com/group/products/rolling-bearings/ball-bearings/deep-groove-ball-bearings/productid-6206

[16] H. Huang, Z. Yuan, W. Kang, Z. Xue, X. Chen, C. Yang, Y. Ye, J. Leng, (2014) Study of the sealing performance of tubing adapters in gas-tight deep-sea water sampler, Int. J. Nav. Archit. Ocean Eng. 6 749–761. doi:10.2478/IJNAOE-2013-0212.

[17] M.B. Davanageri, S. Narendranath, R. Kadoli, (2018) Finite Element Wear Behaviour Modelling of Super duplex stainless steel AISI 2507 Using Ansys, IOP Conf. Ser. Mater. Sci. Eng. 376. doi:10.1088/1757899X/376/1/012131.

[18] L. Gardner, The use of stainless steel in structures, Prog. Struct. Eng. Mater. 7 (2005) 45–55. doi:10.1002/pse.190.

[19] Grunwald, B., (2018) Vibration analysis of shaft in SolidWorks and ANSYS.

[20] Mansoora, H.I., M. Al-Shammari, and A. Al-Hamood. (2020) Theoretical Analysis of the Vibrations in Gas Turbine Rotor. in IOP Conference Series: Materials Science and Engineering. IOP Publishing